Listening to Turbulence: Measuring Coherence Decay at Different Positions on an Aircraft in Cruise Flight

Stefan Haxter* and Carsten Spehr†

German Aerospace Center DLR, D-37073 Göttingen, Germany

The coherence lengths underneath a turbulent boundary layer were measured in flight at several positions on an aircraft. It was found that the coherence length scales with the boundary layer thickness, except for one measurement position where the boundary layer was believed to be disturbed by the vicinity of the wing. A comparison of the data with the models by Corcos and Efimtsov showed an underprediction of the values. However good applicability of the Efimtsov-theory was found when fitted to the measured data. A variation of flight speed and flight altitude showed no considerable change in the coherence length parameters. Variation of interior sound level is therefore not ascribed to a variation of coherence length, but rather to a variation of other parameters.

I. Introduction

Sufficiently accurate prediction of the boundary layer excitation of aircraft panels at cruise flight conditions is still an open issue in aero-vibro acoustics. The present procedure for prediction can be split into two parts: the first addresses measuring and statistically describing or modeling the excitation behavior of the boundary layer,[1,2,3,4] while the second part deals with how the underlying airframe structure is likely to be excited.[5,6,7]

This article focusses on the first part - measurement and statistical description of the excitation behavior of the boundary layer. More precisely, the focus of this article is to determine the influence of measurement position onboard the aircraft on the pressure fluctuation characteristics of the boundary layer.

One important characteristic for the determination of the excitation behavior of the boundary layer is the decay of coherence of turbulent structures in the boundary layer. A model for the prediction of this decay was published by Efimtsov.[2] A feature of the model is the Strouhal-Number-dependent prediction of coherence length, which is a measure of over what distance the turbulent structures still show a certain amount of similarity. In contrast to the preceding Corcos model,[1] the Efimtsov model limits the maximum value of this coherence length depending on the boundary layer thickness. The Efimtsov model is derived from flight test data in the sub- and supersonic range. However, in the paper published by Efimtsov, no information is given about the measurement setup and the flight conditions used.

In current research by the authors[8,9] and by Palumbo,[10] flight test data at cruise flight altitudes and speeds were investigated. In the authors' investigation, the transducer array was positioned in the center of the aircraft in the vicinity of the wing. Due to the design of the array it was possible to analyze the influence of variation of speed and altitude on the coherence length separately. No considerable influence of speed was found. The variation of altitude indicated a small effect on the maximum coherence length which is limited by the boundary layer thickness. However, the Efimtsov model was found to under predict the coherence length values at this measurement position.

In the measurement of Palumbo, the position of the transducer array was in the front of the aircraft. The coherence length values from that measurement exceed the Efimtsov prediction by an even greater extent.

Even the two recent measurements by the authors and by Palumbo show considerable difference in their measured coherence length values. As indicated by Palumbo[11] this difference is caused by the different

*PhD student, Institute of Aerodynamics and Flow Technology - Experimental Methods, stefan.haxter@dlr.de, member AIAA

†Research Engineer, Institute of Aerodynamics and Flow Technology - Experimental Methods, carsten.spehr@dlr.de, member AIAA

positioning of the array in the aircraft. Therefore, the aim of this paper is to determine the influence of measurement position onboard the aircraft on the coherence lengths. Measurements at constant speed, altitude, and with the same aircraft type are used, with only the array position being varied throughout the different flights.

II. Measurement Setup

Flight test data were acquired in three measurement campaigns using the DLR's model A320 Advanced Technology Research Aircraft (ATRA). A more detailed description of the first test can be found in reference 12. The first campaign was conducted in May 2011, the second one in September 2012 and the third one in October 2012. In each test, three aluminum dummy windows were installed in three adjacent window banks on the right hand side of the aircraft. The absolute position of these three window banks was changed in each campaign: in the first campaign, the windows were located in the vicinity of the wing, in the second campaign, they were located in the aft section of the aircraft and in the third campaign, the first three available window banks were used for positioning. The position of the array is sketched in figure 1. Boundary layer run lengths to the center of the three-window-array are summarized in table 1.

Figure 1. Positioning of the three-window transducer array on the ATRA

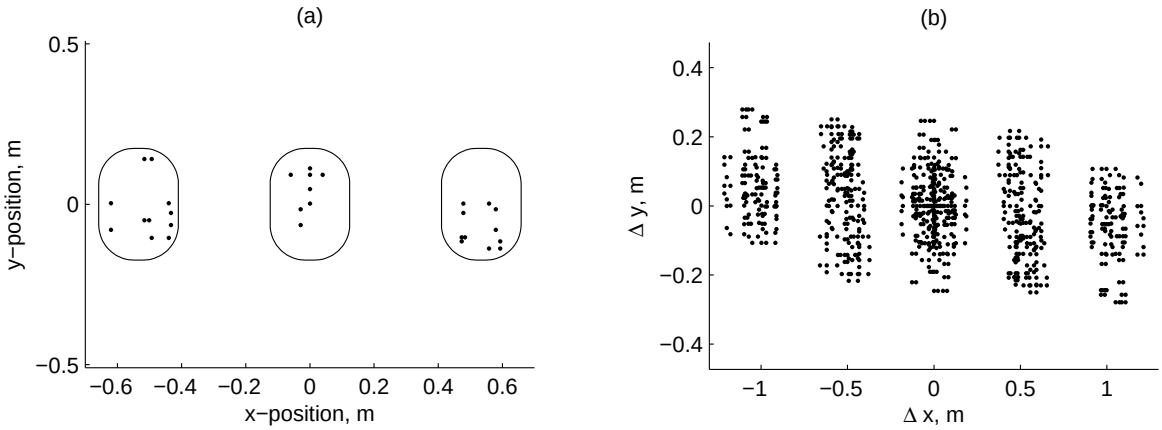

Figure 2. (a) Three-window array with transducer positions; (b) Coarray

Thirty piezo-resistive pressure transducers were installed in a quasi-randomized pattern over the three aluminum windows (figure 2 (a)). The pattern provided one neighbor element at the same lengthwise (aircraft length axis) and crosswise (perpendicular to aircraft length axis on the surface) position. 435

different transducer spacing combinations resulted from this distribution. The minimum and maximum spacings were, respectively, 10 mm and approximately 1.2 m in lengthwise and 13 mm and approximately 28 cm in crosswise direction. All transducer combination spacing positions are called the "co-array". This is displayed in figure 2 (b).

The sampling rate of the signals was 50 kHz. The piezo-resistive transducers produced a small electrical charge as a signal when exposed to pressure. This electrical charge was pre-amplified by an amplifier close to the three-window array. The amplified signal was then routed to the in-flight measurement system. The transducers were pinhole-mounted in order to limit the spatial resolution of each transducer to the area of a hole with 0.3 mm diameter.

Parameters pertaining to the flight environment - such as dynamic pressure, altitude, speed and Mach number - are measured on a regular basis on the aircraft for the instruments on the flight deck; these parameters were read out of the system and recorded synchronously by a basic flight test instrumentation unit.

For the setup of the Efimtsov model, boundary layer parameters such as layer thickness and friction coefficient are needed. These parameters were not measured in flight due to the additional complexity of the needed experimental setup. Therefore boundary layer thickness was estimated using a formula provided by Bies.[13] The procedure was adapted to the flight conditions of a jet airliner by measurement data provided by Gyorgyfalvy[14] who conducted boundary layer thickness measurements on a Boeing 720 Jetliner (single aisle). The original scaling factor of 0.37 was therefore modified to 0.443 by comparing the boundary layer thickness measurements by Gyorgyfalvy to the result of equation (1) when employing the measurement setup used there.

$$\delta_{est.} = 0.443 \cdot x \cdot \mathrm{Re}_x^{-1/5} \cdot \left[1 + \left(\frac{\mathrm{Re}_x}{6.9 \cdot 10^7}\right)^2\right]^{0.1} \tag{1}$$

Gyorgyfalvy also provided an estimation of the surface friction coefficient $c_f = 1.35 \cdot 10^{-3}$, which was used later in this evaluation for the setup of the Efimtsov model.

III. Test Environment

Several flight conditions were selected for analysis. Each flight condition had been measured three times - each with a different array position. The flight conditions selected were located in a plus-shaped pattern that allowed separate variation of flight speed and flight altitude. The nominal positions are displayed as points in figure 3. Each point in the graphs represents three single measurements, each with the same conditions, but with a different array position. A summary of the parameters measured by the basic flight-instrumentation is given in table 1, in which the actual data read out from the flight avionics is presented. Case 4.A was measured at FL260 instead of FL250. However, as will be shown later on, this did not have an influence on the measured coherence length.

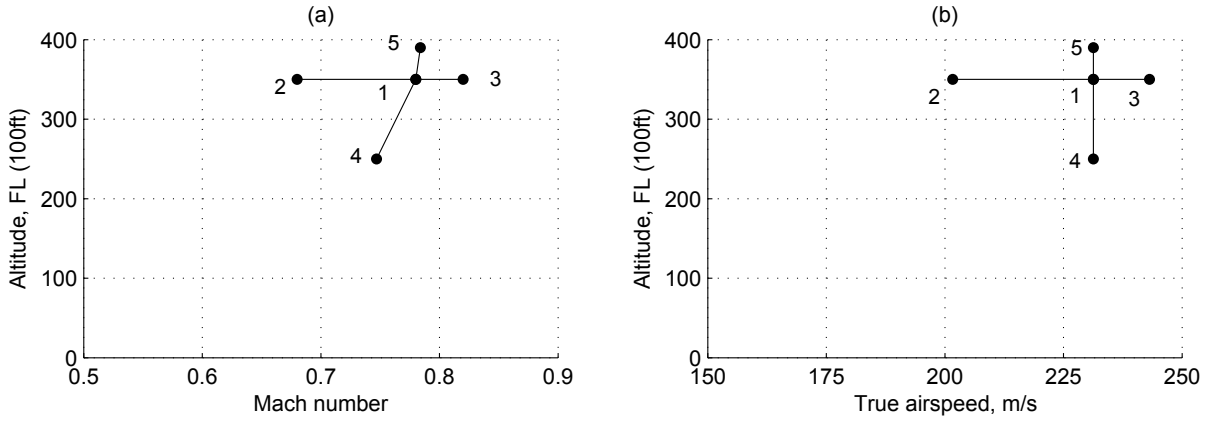

Figure 3. Sketch of targeted flight conditions; displayed in (a) Mach number; (b) true airspeed (TAS)

Index	FL[100ft]	U_∞[m/s]	M	T[K]	p_{stat}[Pa]	x[m]	$\delta_{est.}$[m]	Re_x	Re_δ	t_{meas}[s]
1.A	350	233.6	0.78	225	23536	6.7	0.093	$3.9 \cdot 10^7$	$5.36 \cdot 10^5$	60
1.B	350	231.8	0.78	222	23547	12.6	0.161	$7.5 \cdot 10^7$	$9.51 \cdot 10^5$	60
1.C	350	235.9	0.78	229	23541	23.4	0.287	$1.3 \cdot 10^8$	$1.63 \cdot 10^6$	10.7
2.A	350	201.5	0.68	219	23726	6.7	0.093	$3.6 \cdot 10^7$	$4.98 \cdot 10^5$	60
2.B	350	206.0	0.68	229	23736	12.6	0.163	$6.3 \cdot 10^7$	$8.18 \cdot 10^5$	12.5
2.C	350	205.9	0.68	228	23752	23.4	0.289	$1.2 \cdot 10^8$	$1.45 \cdot 10^6$	15.2
3.A	350	246.8	0.82	225	23470	6.7	0.092	$4.1 \cdot 10^7$	$5.62 \cdot 10^5$	60
3.B	350	246.6	0.82	228	23477	12.6	0.161	$7.5 \cdot 10^7$	$9.60 \cdot 10^5$	60
3.C	350	246.9	0.82	228	23538	23.4	0.287	$1.4 \cdot 10^8$	$1.71 \cdot 10^6$	5.5
4.A	260	233.6	0.76	237	35528	6.7	0.089	$5.3 \cdot 10^7$	$7.04 \cdot 10^5$	12.7
4.B	250	234.1	0.76	238	37128	12.6	0.157	$1.0 \cdot 10^8$	$1.30 \cdot 10^6$	12.6
4.C	250	225.9	0.73	224	37242	23.4	0.284	$1.8 \cdot 10^8$	$2.24 \cdot 10^6$	60
5.A	390	231.6	0.80	211	19429	6.7	0.094	$3.6 \cdot 10^7$	$5.00 \cdot 10^5$	7.4
5.B	390	233.3	0.81	209	19433	12.6	0.162	$6.9 \cdot 10^7$	$8.89 \cdot 10^5$	15.5
5.C	390	234.2	0.79	220	19418	23.4	0.289	$1.2 \cdot 10^8$	$1.44 \cdot 10^6$	20

Table 1. Selected flight conditions for analysis. Data read out from flight avionics. (A): front; (B): mid; (C): aft-section

IV. Data Processing

A. Determination of Cross-Spectra

Averaged cross spectra were calculated as in the first evaluation data of the flight campaign.[9] Both signals of each transducer pairing were transformed into the frequency domain via an averaged Fast Fourier Transform routine by Welch[15] using an overlap factor of 0.5. Before averaging, the Fourier Transforms of each were multiplied with the complex conjugate in order to obtain the cross spectra. A window size of 4096 samples was chosen for transformation which resulted in a frequency bandwidth of $\Delta f = 12.2\,\mathrm{Hz}$. The window size of 4096 samples corresponds to a recorded time of 80 ms. In the literature, convective velocity has been measured to be a fraction greater than 60 % of the flow speed.[16,17] Even if the convective velocity of the turbulent structures in the boundary layer was only 50 % of a low flight velocity of $200\,\mathrm{m\,s^{-1}}$, this would result in a distance of 8 m traveled by the turbulent structures over the duration of each evaluation window. This distance is far greater than the size of the array used and therefore the evaluation window size is presumed to be sufficient to include turbulent structures passing each transducer. This effect has also been addressed by Palumbo[10] who examined the influence of different evaluation window sizes on the cross-spectra of pressure signals recorded a certain distance apart. A Hann window was applied to each block in order to reduce spectral leakage. Using an overlap factor of 0.5 the measurement time of 60 s resulted in a total number of 1431 averages for each cross-spectrum.

B. Determination of coherence lengths

When the coherence is plotted over the coarray, an indication is obtained of how the signals decorrelate spatially due to the loss of identity of the turbulent structures in the boundary layer. Measured coherence lengths from a front installation case are shown for a single frequency of $f = 500\,\mathrm{Hz}$ as black dots in figure 4. In the center of the figure at $\Delta x = \Delta y = 0$ the coherence has a value of one. With increasing distance from the center the signals start to decorrelate. The amount of de-correlation is a directional property: de-correlation in cross-flow direction is more pronounced than in flow direction due to convection of the turbulent structures. A double-exponential fit through the data points is shown in figure 4 as a colored surface. The fit has two parameters: a decay coefficient in longitudinal and a decay parameter in lateral direction. When these two parameters are fitted, the double-exponential is a good approximation of the coherence decay behavior.

The use of an exponential with negative exponent had already been proposed by Corcos.[1] Palumbo used

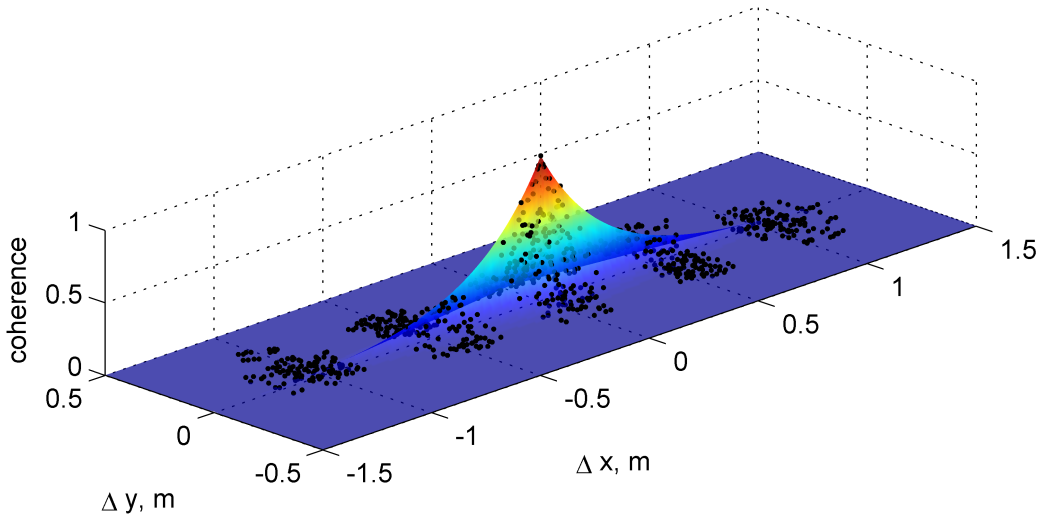

Figure 4. An example of a two-dimensional coherence fit at $f = 500\,\mathrm{Hz}$ in the front section

flight test data to perform the fitting for the longitudinal and the lateral direction separately.[10] In his test, the alignment of the flow direction with the one-dimensional array was achieved in a straightforward way by aligning an outside-attached string on the adjacent downstream passenger window to a marker that was in line with the transducers on the measurement window.

In the present test, the deviation between the flow angle and the aircraft longitudinal axis over the array could be determined from the measured data. Due to the quasi-randomized distribution of the transducers in the array, the transducer spacing combinations in the coarray are not limited to the $\Delta x = 0$ and $\Delta y = 0$ -axis, but rather distributed over the whole spacing domain. Of all these transducer spacings the one with the largest spacing at which a considerable coherence is still present was presumed to be representative of the local flow direction.

In order to reduce an influence of outliers when just taking the largest spacing above a certain threshold as the flow direction, the determination of this direction was achieved by applying a principal component analysis to all spacings above the threshold.[9] All spacings having a coherence value above a threshold of $\exp(-1)$ were taken as input and the analysis delivered the orientation of all these spacings. For frequencies above 2500 Hz, this threshold was lowered to $\exp(-2)$ to reduce misinterpretation resulting from the limited spatial array resolution.

After determination of the flow angle, a two-dimensional fit was applied to the coherence data. The fit consisted of two exponential functions that were aligned orthogonally in the spacing domain. The exponential for the longitudinal coherence decay was aligned with the flow direction determined beforehand. From the fit coherence decay parameters in flow direction l_x and in cross-flow direction l_y were obtained. The fit function is summarized in equation (2).

$$\Gamma(f) = \exp\left(-\frac{\xi}{l_x(f)}\right) \cdot \exp\left(-\frac{\eta}{l_y(f)}\right) \tag{2}$$

When the fitting is complete, the difference between the fit and the actual measured coherence values can be calculated. The magnitude of the difference is representative for the goodness of the exponential fit as a model for the decay of coherence over distance.

The coherence lengths can be approximated by the Efimtsov function

$$l_{x,E} = \delta \left[\left(\frac{a_1 Sh_E}{u_c/u_\tau} \right)^2 + \frac{a_2^2}{Sh_E^2 + (a_2/a_3)^2} \right]^{-1/2} \tag{3}$$

as a function of frequency and the three parameters a_1, a_2 and a_3. Equation (3) contains the Strouhal

number $Sh = \omega\delta/u_\tau$ (mixed scaling), the convective velocity u_c, the friction velocity $u_\tau = \sqrt{\tau/\rho}$, and the three constants $a_1 = 0.1$, $a_2 = 72.8$, and $a_3 = 1.54$. Besides the set of constants a_1, a_2, and a_3 provided by Efimtsov, they can also be determined by experiment. The parameters will be fitted to the measured data in this paper using a RANSAC-method. The curve resulting from the Efimtsov model with adapted parameters will be denoted as "fitted function" throughout the paper.

The Corcos model is given by

$$l_{x,C} = \frac{u_c}{\alpha_x \cdot \omega} \tag{4}$$

in which α is a constant representing the decay. In the literature, values of $\alpha_x \approx 0.1\,\mathrm{m}$ and $\alpha_x \approx 0.01\,\mathrm{m}$ are found.

C. Using Engine-Idle Flight Attitudes

When comparing measurements in the aft-section with the thrust set to a cruise setting to a case with thrust idle it was found that the jet noise from the engine caused a very significant increase in surface pressure fluctuation in the measurement area. The signals caused by the engine noise were correlated over the array. In in contrast to hydrodynamic pressure fluctuations, which result in the blade-like coherence pattern shown in figure 4, the acoustic pressure fluctuations cause a quasi-constant increase of coherence over the whole spacing domain. This is due to the slow decay of acoustic wave correlation in comparison with the correlation of turbulent boundary layer pressure fluctuations. However, if the proportion of correlated pressure fluctuations resulting from acoustic waves is too high, the coherence resulting from the acoustic pressure fluctuations will overlap the hydrodynamic blade-like structure which will then be no longer detectable by means of coherence in the spatial domain. It is possible to use the phase information in the cross-spectra in order to separate acoustical from hydrodynamic pressure fluctuations. However, this will not be done in this paper, but rather measurements with the engine thrust set to idle were used for analysis of the aft-section. At a constant altitude, this resulted in a deceleration of the aircraft speed over measurement time. A portion of the signals where the Mach number of the aircraft was within ± 0.01 of the desired value was taken for analysis and the cross-spectral matrices were calculated for this subrange of the signal only. The time span used for analysis was in the range of 10 s which resulted in approximately 120 averages for the calculation of mean cross-spectra for the aft section measurements. The information about the current flight Mach number was read out from the regular onboard avionic system.

V. Results

In the following, the five cases as presented in figure 3 are discussed separately, one after the other. Afterwards, a summary of the coherence length diagrams is given for both the variation of speed and the variation of altitude.

A. Case 1

In figure 5 the coherence length normalized with the boundary layer thickness for three different positions on the aircraft at flight condition number 1 is shown. The measured points are depicted as red dots. A representative deviation of the exponential fit from the measured coherence decay is shown as black error bars which is sometimes not visible due to the small value of the deviation. The left, middle and right subfigure show, respectively, the coherence lengths from data obtained at the front, at the center and in the aft sections of the aircraft.

When normalized to the boundary layer thickness, this normalized coherence length shows a similar characteristic behavior in the front- mid- and aft-section. The value of l_x/δ starts in the low-Strouhal number region at a relatively high level and increases slightly until a maximum is reached. This maximum is visible best in the mid- and aft-sections at $Sh \approx 0.25$. In the front-section, the occurrence of the maximum is not so pronounced, since l_x/δ at lower Strouhal number is higher than for the mid- and aft-positions. The fact that the position of the maximum is at a fairly constant position when using outer variables for the normalization (i.e. displacement thickness and free-stream velocity), is a hint that the cause for this lies in the limitation of turbulent structure size due to boundary layer thickness. After the maximum, the double-logarithmic plot shows a linear drop of the normalized coherence length with Strouhal number. The boundary layer in the mid-section is considered to be more disturbed than in the front- and aft-sections

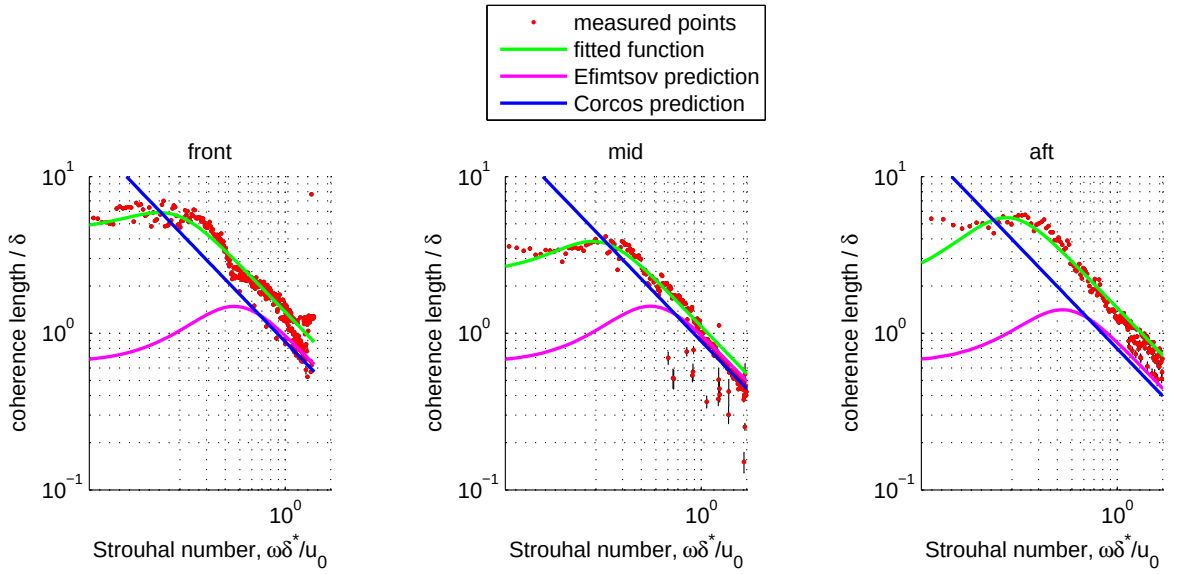

Figure 5. Coherence length resulting from analysis in the front-, mid-, and aft-sections; Case 1: FL350; M=0.78; TAS=234 m s^{-1}

due to its proximity to the pressure field of the wing. The scaling of coherence length with boundary layer thickness - as implemented in the Efimtsov model - is verified by the similar values of normalized coherence length for the two rather undisturbed cases of the front- and aft-sections.

Although the front- and mid-section coherence lengths show a similar behavior at first sight, they do nevertheless exhibit some differences when examined in greater detail. In the front section, the coherence length shows a broadly-shaped peak rather than the more narrow one seen in the mid-section. Also, the drop-off from the maximum coherence length towards higher frequencies in the front section appears to occur as a twofold linear process with a change in slope at $Sh \approx 0.35$. The drop-off from the maximum in the mid-section appears to occur in a more hyperbolic way - in concurrence with the theory of Efimtsov and Corcos. The aft-section shows a slight increase of coherence length at very low Strouhal number (lower than the maximum position).

The results from the Efimtsov model prediction are shown as purple lines in figure 5 for the front-, mid-, and aft-sections. The estimated boundary layer thickness for each position and the estimated value for the friction velocity u_τ in the center of the airplane were used for the application of the model. It can be seen that there is a good agreement of coherence length at different positions when normalized with the boundary layer thickness. The boundary layer thickness increases with distance of the measurement position from the nose. The coherence length therefore increases at the same rate as the boundary layer thickness increases. At higher Strouhal numbers than the one at which the maximum coherence length occurs, the Efimtsov model underpredicts the coherence length values in the front- and in the aft-sections, whereas in the mid-section, the coherence lengths at high Strouhal number are predicted correctly. This is presumed to be influenced by the increased favorable pressure gradient in this region.

The results from the Corcos model are shown in the figures as blue lines as well. As expected, the model does not show any limitation in boundary layer thickness in the low-Strouhal number region. At higher Strouhal numbers, in the mid- and aft-sections, the predicted decay of coherence length is as expected, yet the model predicts values that are lower than the measured values, except for the mid-section.

A fitted Efimtsov model is shown in the figure as well. The Efimtsov model is able to reproduce the behavior of the coherence length over Strouhal number quite well, if the parameters are changed. There is a considerable deviation in the low-Strouhal number behavior at all three positions. The peak shape is reproduced correctly in the mid- and aft-sections while the fit does not cover the peak shape correctly in the mid-section.

B. Case 2

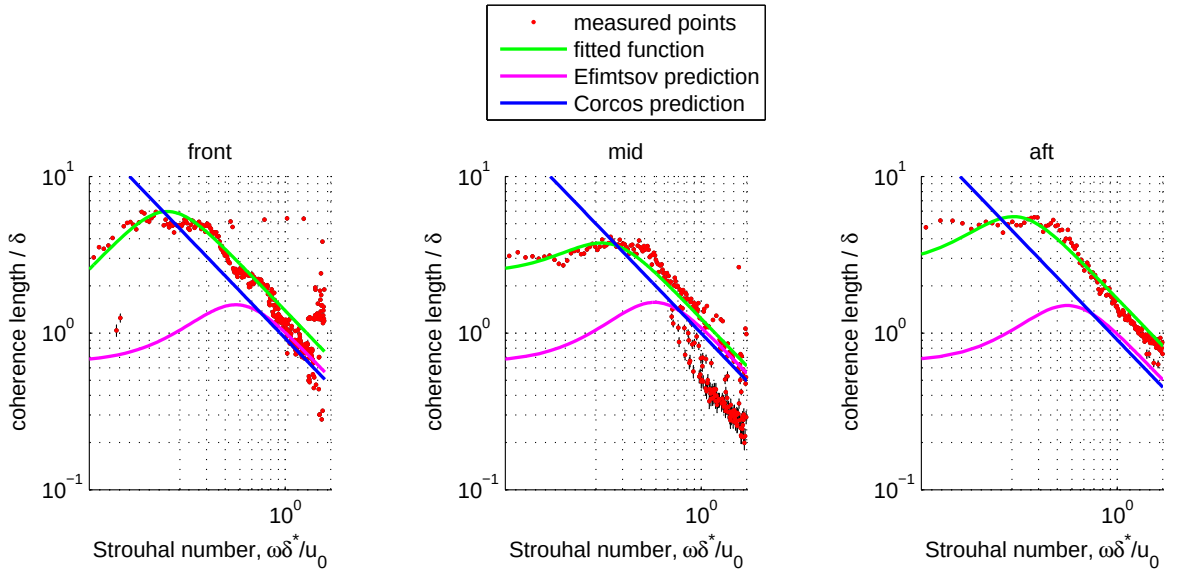

Figure 6. Coherence length resulting from analysis in the front-, mid-, and aft-sections; Case 2: FL350; M=0.68

When the speed is reduced to a Mach number of $M = 0.68$ while maintaining the flight altitude, coherence lengths as depicted in figure 6 are measured. The characteristics of the curves are essentially unaltered compared with the $M = 0.78$-case. In the front-section, the low-Strouhal number behavior is lowered and a maximum coherence length position is clearly visible. In the mid-section the normalized coherence length above a Strouhal number of 1 decreases by a constant offset. This had also been observed for the case at the same altitude but higher flight speed. Again, the front- and aft-sections show a similar maximum value for the normalized coherence lengths. The maximum position has increased slightly to a value of $Sh \approx 0.3$ for the mid- and aft-sections. The position of the maximum in the front-section is observed at a Strouhal number of $Sh \approx 0.15$. The maximum value of the normalized coherence length is approximately $l_{x,max} \approx 6\delta$ in the front- and aft-sections and $l_{x,max} \approx 4\delta$ in the mid-section. Again, at very low Strouhal number, a slight increase of coherence length is visible in the aft-section.

The Efimtsov and Corcos models both underpredict the coherence length values at high frequencies. The Corcos model shows again its non-limited behavior at low Strouhal numbers caused by the absence of a boundary layer limitation, while this limitation of the boundary layer thickness is too strict in the Efimtsov model with its original set of parameters. In the mid section the measured coherence length lies below the prediction above a Strouhal number of $Sh \approx 1$.

When fitted to the measured points, the Efimtsov function is able to reproduce the measurement very well, except at very low Strouhal numbers in the aft section and at high Strouhal number in the mid-section where a constant offset is present.

C. Case 3

For a higher speed at Mach number $M = 0.82$, but still constant flight altitude of $FL350$ the measured coherence length is shown in figure 7. The basic characteristic of the curves is again essentially unaltered, except for little differences. The coherence length in the front-section shows once again a twofold decay process. Also, there is no occurrence of a constant lowering of coherence length in the mid-section at high Strouhal numbers as it was observed in Case 2. The front-section coherence length shows a very broad maximum at low Strouhal number, while the mid- and aft-sections show a maximum at $Sh \approx 0.2$ and $Sh \approx 0.22$, respectively. The maximum value in the front is slightly increased and reaches a value of $l_{x,max} \approx 7\delta$ of maximum coherence length. In the mid- and aft-sections the maximum values are again

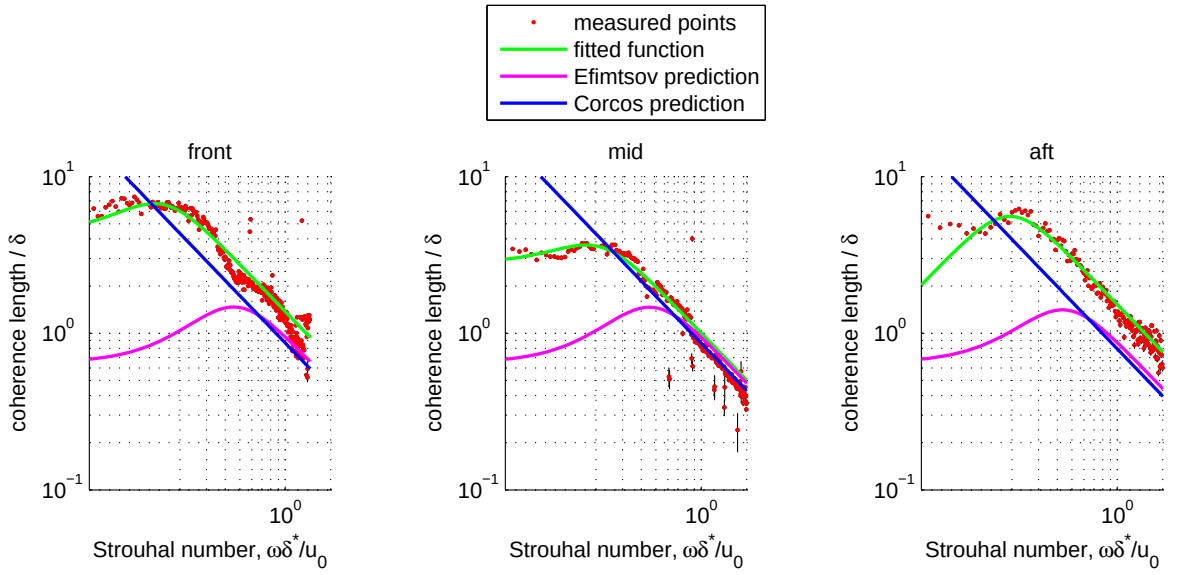

Figure 7. Coherence length resulting from analysis in the front-, mid-, and aft-sections; Case 3: FL350; M=0.82

at $l_{x,max} \approx 4\delta$ and $l_{x,max} \approx 6\delta$ respectively. A slight increase of coherence length is again visible in the aft-section at very low Strouhal number.

The Efimtsov and Corcos prediction are again too low in the high-Strouhal number region for the front- and aft-sections. In the mid-section, the values at high Strouhal numbers are predicted correctly. As before, the boundary layer limitation of the original Efimtsov model is too strict and predicts a maximum value that is too low.

D. Case 4

Reducing the flight altitude compared to Case 1, but leaving the flow speed constant gives the coherence lengths shown in figure 8. At the lower altitude, the maximum coherence length is slightly increased in the front-section compared to Case 1. In the mid- and aft-sections, the maximum values appear to be slightly lower than in Case 1 at higher altitude. The maximum position increases from $Sh \approx 0.18$ in the front-section to $Sh \approx 0.2$ in the mid- and $Sh \approx 0.22$ in the aft-section. A drop of coherence length is once again observed in the mid-section at Strouhal numbers greater than $Sh \approx 0.6$. In the front-region, the coherence length above a Strouhal number of $Sh \approx 0.6$ appears to be disturbed, with the values showing a greater spread.

The Corcos and Efimtsov model underpredict the coherence length values in the front- and aft sections in the drop-off region at higher Strouhal number. In the front-case difference is not so pronounced due to the increased spread of the values. The boundary layer thickness limitation implied by the original Efimtsov model is again too strict.

E. Case 5

Still at a constant speed, but at the highest flight altitude under consideration, the coherence lengths measured in case 5 are shown in figure 9. Here, the coherence length in the front-section shows a broad peak with a maximum value of $l_{x,max} \approx 7\delta$ at $Sh \approx 0.15$. The peak is lowered again in the mid-section and shifted to a slightly higher Strouhal number. In the aft-section, the peak value is restored to $l_{x,max} \approx 6\delta$ at $Sh \approx 0.22$. At this flight attitude, the coherence length in the front-section shows a behavior that differs slightly from the previous cases: starting at the maximum position, the measured coherence length drops very sharply and reaches the predicted values at approximately $Sh \approx 0.6$. From here, the coherence length decays at the regular rate in concurrence with the predicted values. The sharp drop is not matched by the

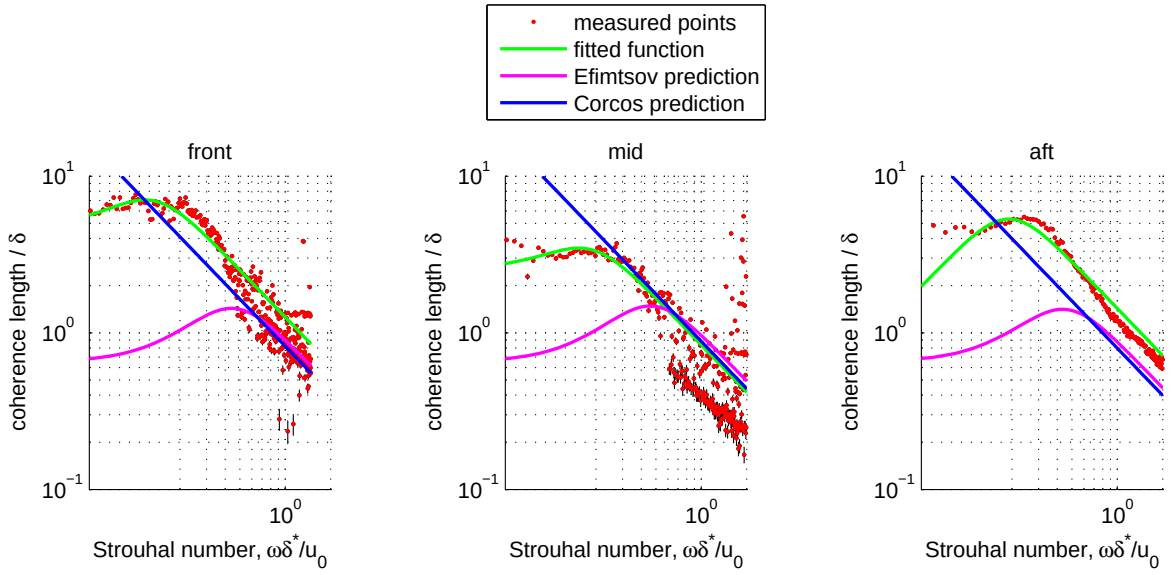

Figure 8. Coherence length resulting from analysis in the front-, mid-, and aft-sections; (c) aft section; Case 4: FL250; TAS=234 m s^{-1}

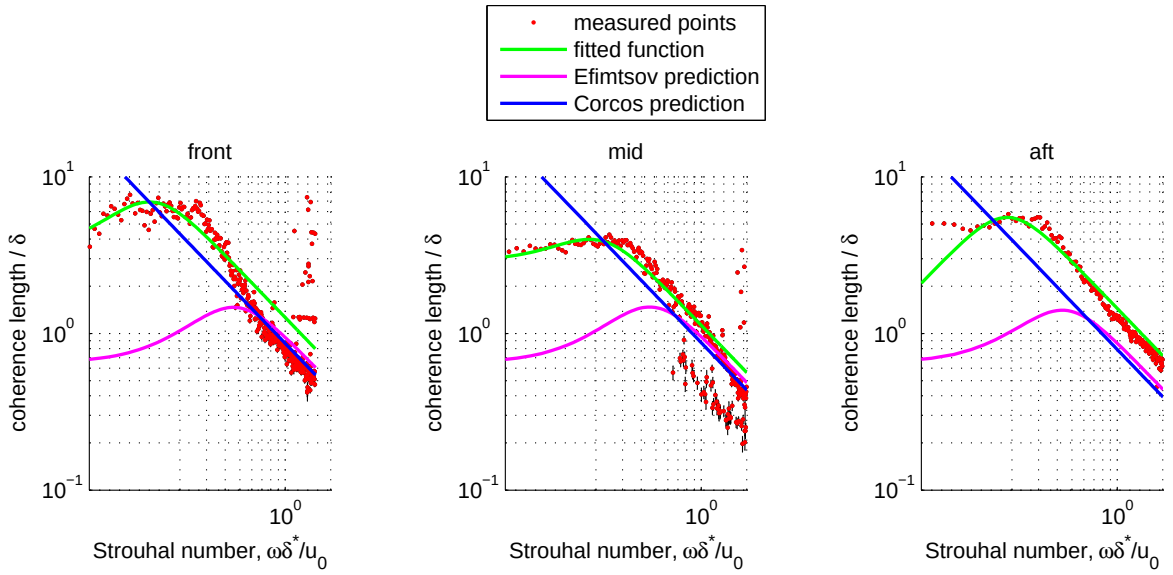

Figure 9. Coherence length resulting from analysis in the front-, mid-, and aft-sections; (c) aft section; Case 5: FL390; MTAS=234 m s^{-1}

fitted curve shown in green. In the aft-section, the slight increase of coherence length at very low Strouhal number is observed, as in the Cases 1,2, and 3.

F. Variation of Speed

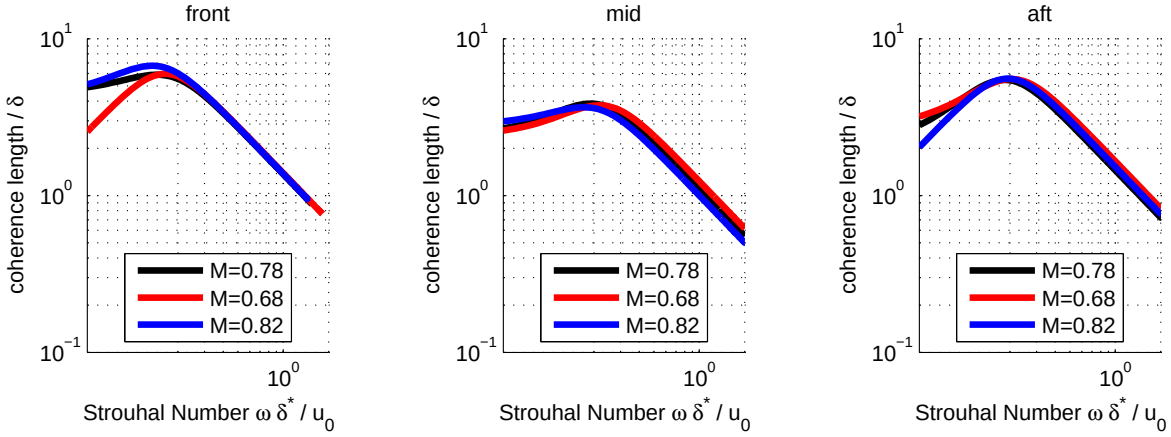

Figure 10. Variation of speed; each measurement position in one plot

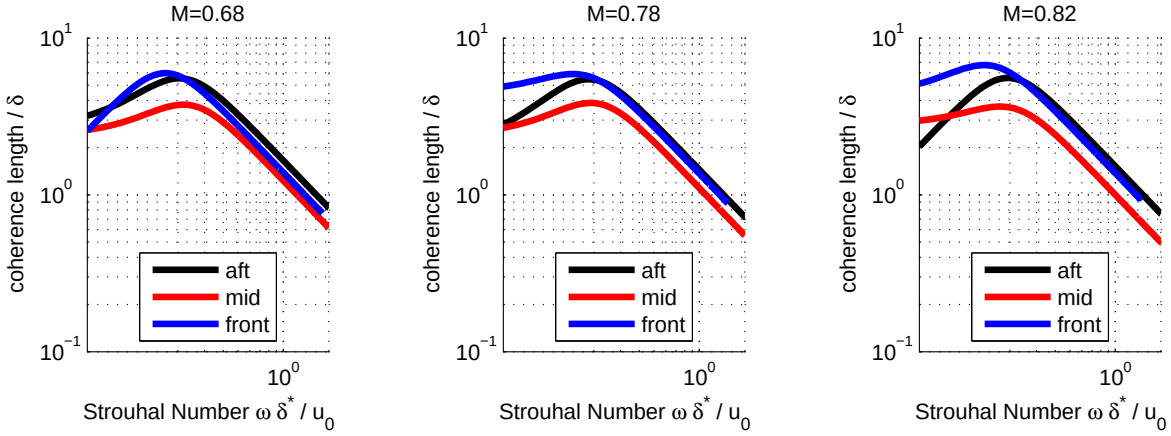

Figure 11. Variation of speed; each speed in one plot

The fitted curves from measurements at constant altitude and variation of speed are shown in figure 10. The overall variation of normalized coherence length with changing speed is very small when compared to the variation of coherence length with measurement position. At all speeds, the normalized coherence length reaches a maximum value of $l_{x,max} \approx 6\delta$ up to $l_{x,max} \approx 7\delta$in the front-section and $l_{x,max} \approx 6\delta$ in the aft-section. In the mid-section, this maximum value is reduced to $l_{x,max} \approx 4\delta$. The position at which the maximum occurs is found to increase slightly with Strouhal number. However, it is pointed out that the boundary layer thickness used for the determination of the Strouhal number and for the normalization of coherence length was estimated and not measured. This is believed to be the cause for the slight variation of the maximum coherence length value and the maximum position in the front- and aft-sections.

In figure 11, the plots are arranged differently in order to show the effect of position at each Mach number. The $M = 0.68$-Case and the $M = 0.78$-Case show very well the deviation of the coherence length measured in the mid-section from the front- and aft- measurements. At $M = 0.82$, the maximum in the aft-section deviates a little from the front-section case, but the high-Strouhal number behavior is essentially similar between the front- and aft-Case. An estimated boundary layer thickness that is too low in the aft-section would have such an effect on the normalized display of coherence length.

G. Variation of Altitude

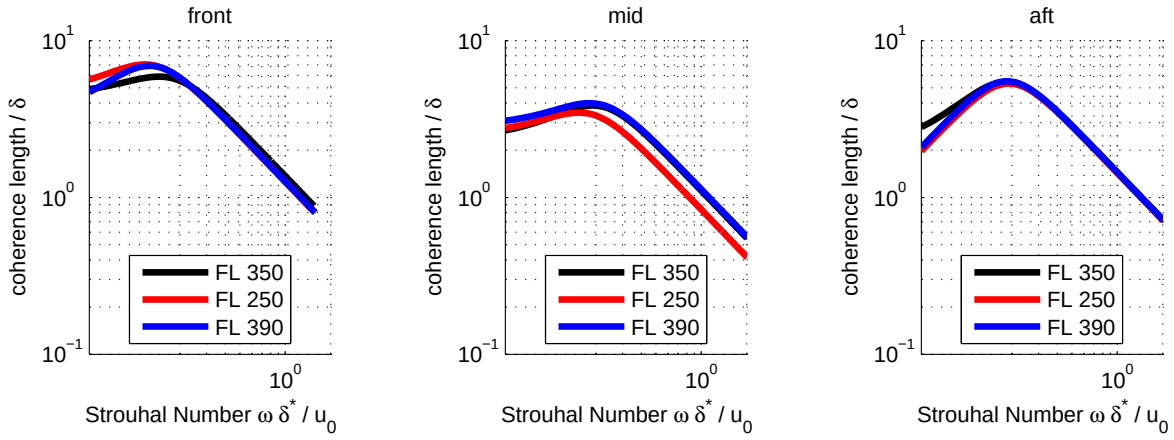

Figure 12. Variation of altitude; each measurement position in one plot

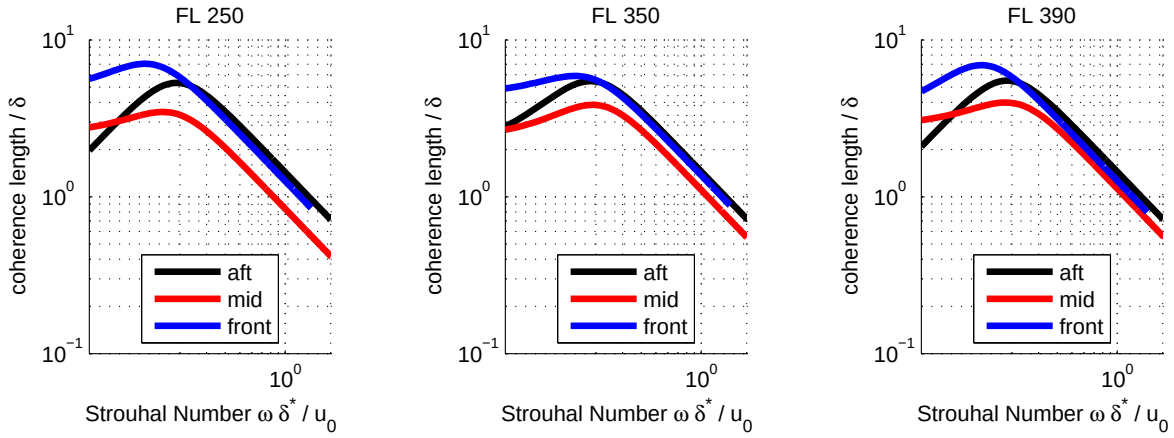

Figure 13. Variation of altitude; each altitude in one plot

The fitted curves from measurements at constant flight speed while changing the flight altitude are shown in figure 12. Again, the overall variation in the plots depends on the measurement position. The fitted curves in the front-section show a similar drop-off (keeping in mind the deviation from this at flight level 390) and the maximum varies slightly, but in a non-systematic manner: While the behavior of the coherence length at the medium flight altitude FL350 is comparable to the aft-section measurements, the maximum of the fit is slightly increased for the lower and higher altitude. In the mid-section, the lowest altitude shows a slight decrease of amplitude together with a slight shift towards smaller Strouhal numbers. In the aft-section the curves for all three altitudes show very good agreement.

Again, plots are arranged differently to show the effect of measurement position. The plot at FL350 shows a coincidence of the front- and aft-section case while the mid-section has a lower level. In the cases at FL250 and FL390, the front-section case shows a higher normalized value than in the aft-section case. This is again assumed to originate in an imprecise boundary layer thickness prediction.

VI. Summary of the results

The findings can be summarized in the following points:

- The front- and aft-sections show similar maximum values of the coherence length when normalized with the boundary layer thickness.

- The normalized coherence length in the mid-section is lower by a facter of 2/3 in comparison with the front- and aft-sections.
- The peak position is similar for all cases and sections with a slight shift towards higher Strouhal number with increased distance from the nose
- The Efimtsov and Corcos model underpredict the coherence length values in the high Strouhal number regions for most cases.
- The boundary layer limitation of the Efimtsov model is too strict when the original parameters are used
- The Efimtsov model function can be fitted very well to describe the behavior of coherence length of Strouhal number.
- A dropoff of coherence length is observed at higher Strouhal numbers in the mid-section
- The correspondance of data, when plotted over the Strouhal number using the boundary layer thickness and free-stream velocity for normalization, has constant deviation throughout the measurement. This is a hint that the boundary layer was not estimated correctly.
- Therefore, the collapse of data using the boundary layer thickness for the coherence length and for the setup of the Strouhal number is believed to be applicable
- The coherence length shows a second little increase at Strouhal numbers below the maximum in the aft-section measurements

VII. Discussion

The results show that the coherence length does change significantly with a variation of position on the aircraft fuselage. This is in accordance with the models used for comparison. When changing flight speed or flight altitude, the coherence length does not change significantly. Hu[18] described an increase of interior noise level when the flight speed is increased, which is therefore not caused by a variation of coherence length. Observations by Spehr et. al.[12] rather suggest a variation of the transfer characteristic of the aircraft hull at different flight speeds.

An increase in flight speed results in an increase of the convection velocity of the turbulent structures in the boundary layer. When displayed in the wavenumber domain (as for instance shown by Bull[19]) the increase of convection velocity shifts the convective ridge in the wavenumber domain towards a smaller wavenumber where the excitation properties of the aircraft panels might be more receptive for energy from the turbulent boundary layer.[20] The shape of the convective ridge stays the same which is to be expected due to the similar coherence lengths with variation of speed.

The coherence lengths were normalized to the boundary layer thickness in the analysis. However, the non-normalized values are relevant for the excitation process. Nevertheless, the boundary layer thickness varies only slightly with variation of altitude and speed as shown in table 1. Therefore, the normalization of the coherence length with the boundary layer thickness plays only a minor role when the excitation potential is compared for the different cases. Still, the necessity of estimating the thickness of the boundary layer is considered to be a open issue. This is especially the case in the vicinity of the wing, where the flow is accelerated and the estimation might not be applicable. Lowson stated that coherence decay might be intensified at high Mach numbers on a surface, which is assumed to occur in the vicinity on the upper side of the wing. However, Lowson[21] states that his findings only apply to the high-frequency part of the coherence decay. The current findings however imply an increased decay throughout the spectrum which then might be caused by normalization to a boundary layer thickness that is not correct.

The lowering of coherence length at high Strouhal number is an interesting feature of the data in the mid-section. It had been denoted by Haxter&Spehr[9] that the flow direction in the vicinity of the wing was not homogenous throughout all frequencies. The flow direction of turbulent structures at high frequency deviate more than for low-frequency structures. The loss of identity of turbulent structures might then be caused by them moving away from the measurement surface due to the curvature of the surface. This behavior was also mentioned by Bhat,[22] who, however, linked this behavior to the low-Strouhal number range.

VIII. Conclusion

Measurements of the coherence length were conducted on an airbus A320 aircraft in the front-section, in the mid-section and in the aft-section of the aircraft. It was found that the coherence lengths increase for all frequencies with increasing distance from the nose of the aircraft to the measurement position. The boundary layer thickness was therefore used for normalization and a good conformity of the data was found when using the Strouhal number based on the boundary layer thickness and the free-stream velocity. The measurement in the mid-section deviated from this behavior, since the coherence length values normalized with the boundary layer thickness were only 2/3 of the values in the front- and in the aft-sections. The reason for this was assumed to be caused by a higher speed of the flow in the vicinity of the wing which either results in a thinner boundary layer than assumed, or a faster decay of the turbulent structures.

A variation of flight altitude and speed showed only very little variation of the coherence lengths at each position of the aircraft. It is therefore concluded that a variation of the transfer characteristic is not caused by a variation of coherence length, but rather by variation of other parameters like the density of outside air when varying altitude, or the convective velocity of turbulent structures in the boundary layer when varying speed.

IX. Acknowledgements

The authors would like to thank the following institutions for their assistance:

- The Federal Ministry of Economics and Technology (BMWi) for the financial support of "SIMKAB" (Simplified Cabin) as part of the aerospace research program (LuFO IV).
- Airbus S.A.S. for the provided infrastructure and help on modifications of the test carrier.
- The DLR Institute of Aeroelasticity, DLR Institute of Flight Systems, and the DLR Flight Experiment team for the help provided in the preparation and performance of the flight test.

References

[1]Corcos, G. M., "Resolution of Pressure in Turbulence," *The Journal of the Acoustical Society of America*, Vol. 35, No. 2, 1963, pp. 192–199.

[2]Efimtsov, M., "Characteristics of the Field of Turbulent Pressures at the Wall of a Boundary Layer," *Sov. Phys. Acoust.*, Vol. 28, No. 4, 1982, pp. 289–292.

[3]Smol'yakov, A. and Tkachenko, V., "Model of a Field of Pseudosonic Turbulent Wall Pressures and Experimental Data," *Akust. Zh.*, Vol. 37, November-December 1991, pp. 1199–1207.

[4]Chase, D., "The character of the turbulent wall pressure spectrum at subconvective wavenumbers and a suggested comprehensive model," *Journal of Sound and Vibration*, Vol. 112, No. 1, 1987, pp. 125 – 147.

[5]Graham, W., "Boundary Layer Induced Noise In Aircraft, Part I: The Flat Plate Model," *Journal of Sound and Vibration*, Vol. vol. 192, part 1, 1996, pp. pp. 101–120.

[6]Graham, W., "Boundary Layer Induced Noise In Aircraft, Part II: The Trimmed Flat Plate Model," *Journal of Sound and Vibration*, Vol. vol. 192, part 1, 1996, pp. pp. 121–138.

[7]Liu, B., "Noise radiation of aircraft panels subjected to boundary layer pressure fluctuations," *Journal of Sound and Vibration*, Vol. vol. 314, 2008, pp. pp.693–711.

[8]Haxter, S. and Spehr, C., "Examination of the Influence of Flight Altitude and Speed on the Efimtsov Model Parameters," *19th AIAA/CEAS Aeroacoustics Conference, Berlin, Germany*, AIAA, May 2013.

[9]Haxter, S. and Spehr, C., "Two-Dimensional Evaluation of Turbulent Boundary Layer Pressure Fluctuations at Cruise Flight Condition," *18th AIAA/CEAS Aeroacoustics Conference, Colorado Springs, Colorado*, AIAA, June 2012.

[10]Palumbo, D., "Determining correlation and coherence lengths in turbulent boundary layer flight data," *Journal of Sound and Vibration*, Vol. 331, No. 16, 2012, pp. 3721 – 3737.

[11]Palumbo, D., "Deriving Lifetime Maps in the Time/Frequency Domain of Coherent Structures in the Turbulent Boundary Layer," Tech. Rep. TM-2008-0023921, NASA, 2008.

[12]Spehr, C., Hennings, H., Buchholz, H., Bouhaj, M., Haxter, S., and Hebler, A., "In-flight sound Measurements: A first overview," *18th AIAA/CEAS Aeroacoustics Conference, Colorado Springs, Colorado*, AIAA, June 2012.

[13]Bies, D. A., "A Review of Flight and Wind Tunnel Measurements of boundary Layer Pressure Fluctuations and Induced Structural Response," Tech. Rep. 29134, NASA, 1966.

[14]Gyorgyfalvy, D., "Effect of Pressurization on Airplane Fuselage Drag," *Journal of Aircraft*, Vol. 2, No. 6, 1965, pp. 531–537.

[15]Welch, P. D., "The use of fast Fourier transform for the estimation of power spectra: A method based on time averaging over short, modified periodograms," *Audio and Electroacoustics, IEEE Transactions on*, Vol. 15, No. 2, 1967, pp. 70–73.

[16]Farabee, T. M. and Casarella, M. J., "Spectral features of wall pressure fluctuations beneath turbulent boundary layers," *Physics of Fluids A: Fluid Dynamics*, Vol. 3, No. 10, 1991, pp. 2410–2420.

[17]Ehrenfried, K. and Koop, L., "Experimental study of pressure fluctuations beneath a compressible turbulent boundary layer," *AIAA 2008-2800*, 2008.

[18]Hu, N., Buchholz, H., Herr, M., Spehr, C., and Haxter, S., "Contributions of different aeroacoustic sources to aircraft cabin noise," *Proceedings of the 19th AIAA/CEAS Aeroacoustics Conference, Berlin, Germany*, 2013.

[19]Bull, M., "Wall-pressure Fluctuations Beneath Turbulent Boundary Layers: Some Reflections On Forty Years Of Research," *Journal of Sound and Vibration*, Vol. vol. 190, part 3, 1996, pp. pp. 299–315.

[20]Rocha, J. and Palumbo, D., "On the sensitivity of sound power radiated by aircraft panels to turbulent boundary layer parameters," *Journal of Sound and Vibration*, Vol. 331, No. 21, 2012, pp. 4785 – 4806.

[21]Lowson, M. V., "Prediction of boundary layer pressure fluctuations," Tech. rep., DTIC Document, 1968.

[22]Bhat, W., "Flight Test Measurement of Exterior Turbulent Boundary Layer Pressure Fluctuations on Boeing Model 737 Airplane," *Journal of Sound and Vibration*, Vol. vol. 14, No. 3, 1971, pp. pp. 439–457.